

# Deep Analysis of CNN Settings for New Cancer Whole-slide Histological Images Segmentation: The Case of Small Training Sets

Sonia Mejbri<sup>1</sup>, Camille Franchet<sup>2</sup>, Reshma Ismat-Ara<sup>1</sup>, Josiane Mothe<sup>1</sup>,  
Pierre Brousset<sup>2</sup> and Emmanuel Faure<sup>1</sup>

<sup>1</sup>Toulouse Institute of Computer Science Research, Toulouse, France

<sup>2</sup>The University Cancer Institute Toulouse, Oncopole, France

**Keywords:** Breast Cancer, Histological Image Analysis, Convolutional Neural Networks, Deep Learning, Semantic Segmentation.

**Abstract:** Accurate analysis and interpretation of stained biopsy images is a crucial step in the cancer diagnostic routine which is mainly done manually by expert pathologists. The recent progress of digital pathology gives us a challenging opportunity to automatically process these complex image data in order to retrieve essential information and to study tissue elements and structures. This paper addresses the task of tissue-level segmentation in intermediate resolution of histopathological breast cancer images. Firstly, we present a new medical dataset we developed which is composed of hematoxylin and eosin stained whole-slide images wherein all 7 tissues were labeled by hand and validated by expert pathologist. Then, with this unique dataset, we proposed an automatic end-to-end framework using deep neural network for tissue-level segmentation. Moreover, we provide a deep analysis of the framework settings that can be used in similar task by the scientific community.

## 1 INTRODUCTION

Cancer is still a leading cause of death worldwide. The detection of breast cancer at an early stage of its development can help to treat it more easily and prevent the progression of the tumor. It is thus of huge importance (Torre et al., 2016). When a suspicious lesion is detected in the breast during a physical examination or a mammogram, additional tests are needed to determine whether it is a cancer or not and, if so, which kind of cancer it is. During biopsy, pathologists examine histological structures in order to provide an accurate diagnosis and several prognostic clues. Practically, pathologists need not only to observe the entire tissue slide at low magnification but also to navigate through different resolutions to be able to combine architectural and cytological information in order to produce their medical diagnosis. This process requires a lot of time and concentration and can be hampered by some inter and intra-individual variability (Loukas, 2013).

Latest technological advances in whole slide imaging and the availability of considerable computational power have enabled digitizing pathology slides at microscopic resolution. This process makes pos-

sible the evaluation of breast cancer stained sections helped by computer vision. These approaches can guide some of the diagnostic routine tasks in order to assist pathologists in the medical decision-making process. This assistance can reduce the workload of the experts by saving time, reducing costs and, most importantly, improving diagnostic (Cruz-Roa et al.; Janowczyk and Madabhushi, 2016). In the context of breast cancer, several machine learning algorithms have been developed and applied to increase the effectiveness in pathological tasks. For instance, researchers have proposed methods to detect nuclei, mitosis (Janowczyk and Madabhushi, 2016) and lymphocytes (Janowczyk and Madabhushi, 2016). These previous studies show several limitations that we address in this work. First, images used in the cited approaches are only small samples of breast cancer or Tissue Micro Arrays (TMA) histological images at full resolution (Beck et al., 2011). Each image captures only a small sample of the full tumor extent, which is not representative of the whole slides images (WSIs) used in routine diagnostic pathology. This problem has partially been addressed by distinguishing tumor-patches from non-tumor-patches (Wang et al., 2016). Another limitation is that related

work studies consider two categories of tissue only (tumor and non tumor) which is not representative of the complex structure of histological images. A typical section of solid tumor is a very heterogeneous structure. Also a single sub-type of breast cancer carcinoma which is Invasive carcinoma (IC) (Cruz-Roa et al.). Previous studies do not take into account the non-invasive breast cancer type called "in situ carcinoma" despite its frequency (20 to 25% of newly diagnosed breast cancers). Reporting the presence of both invasive and/or in situ carcinoma is a challenging part of a diagnostic pathology workup since there is a significant difference of treatment options of the disease. It might be crucial to identify areas where a full resolution analysis should be performed. There are very few whole slide breast cancer datasets with pixel-level annotations. Regarding breast cancer pathological dataset Spanhol *et al* introduced The Breast Cancer Histopathological Image Classification (BreakHis) which is composed of 2,480 benign and 5,429 malignant samples of microscopic images of breast tumor tissue (Spanhol et al.). However, these two categories of tissues are not enough because it does not reflect the complexity of tissue diversity. To tackle this shortcoming, Grand Challenge on Breast Cancer Histology Images (BACH) had launched an annotated Whole-slide images dataset (Aresta et al., 2018). The organization provided 10 pixel-wise annotated regions for the benign, in situ and invasive carcinoma classes present in a entire sampled tissue which represent a partially annotated masks. In recent years, deep learning models, especially convolutional neural networks (CNNs) (LeCun et al.) have emerged as a new and more powerful model for automatic segmentation of pathological images. The power of a CNN based model lies in its deep architecture which allows for learning relevant features at lower levels of abstraction. (Hou et al., 2016) proposed a patch-based CNN and to train a decision fusion model as a two-level model: patch-based and image-based model to classify WSIs into tumor subtypes and grades. Chen *et al.* proposed an encoder-decoder architecture to gland segmentation in benign and malignant (Chen et al., 2016a). Cruz *et al.* presented a classification approach for detecting presence and extent of invasive breast cancer on WSIs using a ConvNet classifier (Cruz-Roa et al.).

The greatest challenge in the medical imaging domain especially in pathology is to deal with small datasets and limited amount of annotated samples, especially when employing supervised convolutional learning algorithms that require large amounts of labeled data for the training process. Previous studies that investigated the problem of breast cancer patho-

logical images analysis, did not provide a proper quantitative and qualitative parameters evaluation for training deep CNN from scratch with few annotated samples only.

## Contributions

The contribution of this paper is two folds: first since there is no publicly available annotated data for this task we developed a new dataset; second we conducted a set of experiments to evaluate several CNN architectures and settings on that new type of data. More precisely, we:

- developed a new dataset of WSIs with different subtypes of breast cancer. The data set consists in 11 whole-slide images fully annotated.
- proposed a fully automatic framework. We applied machine learning algorithms to extract the predictive model, and more precisely, we applied and adapted a patch-based deep learning approach on our new dataset. While our model relies on existing architectures (SegNet (Badrinarayanan and Kendall, 2017), U-Net (Ronneberger et al.), FCN (Long et al., 2015) and DeepLab (Chen et al., 2016b)), the originality of our work resides in a deep analysis of the parameters of the model.
- conducted several experiments to evaluate the settings of each step of the proposed framework in order to get the optimal set of parameters when dealing with this new data for a tissue-level segmentation task.

The paper is organized as follows: in Section 2, we present the new data set that we built. Section 3 presents the framework we developed as well as an overview of the experiments and evaluation measures. Section 4 presents the details of the experiments and their results. Section 5 provides the main recommendations related to the influence of the model parameters. Section 6 concludes this paper and discusses future work.

## 2 NEW ANNOTATED DATASET

This work involved anonymized breast cancer slides from the archives of the pathology department of the Toulouse University Cancer Institute. The breast cancer images were acquired with a Panoramic Digital Slide Scanners 3DHISTECH. This selection was reviewed by an expert pathologist to confirm the presence of at least one of the two cited categories of carcinoma considered in this study. To describe the complexity of the tissue structures present in the image

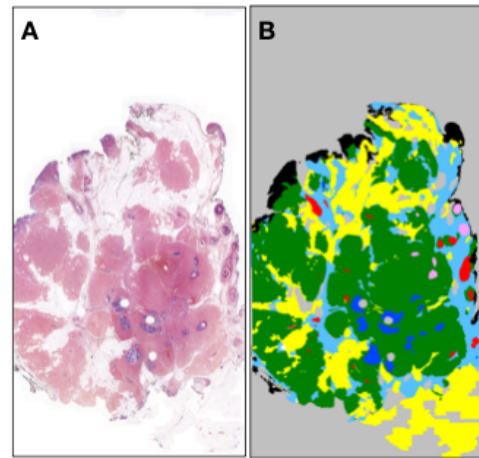
Table 1: Tissues categories characteristics and corresponding average area present in the dataset.

Tissue label	Avg. area	Tissue description
Invasive carcinoma (IC)	8.11% ( $\pm 7.2\%$ )	carcinoma that spreads outside the ducts and invade the surrounding breast tissue.
Ductal Carcinoma <i>In situ</i> (DCIS)	0.75% ( $\pm 1.89\%$ )	carcinoma confined to the ducts.
Benign epithelium	1.77% ( $\pm 1.9\%$ )	non-malignant lesions in the tissue.
Simple stroma	18.57% ( $\pm 8.58\%$ )	homogeneous composition, includes tumor stroma and fibrosis
Complex stroma	8.57% ( $\pm 6.2\%$ )	heterogeneous composition, a mixture of fibrous and adipose tissue
Adipose tissue	21.5% ( $\pm 11.31\%$ )	monotonous tissue, comprised mostly of adipocytes, fat-storing cells.
Artifacts	1.15% ( $\pm 1.09\%$ )	random noise due to the staining procedure and folds of tissue slices
Background	43.96% ( $\pm 8.53\%$ )	absence of tissue

of breast cancer, the pathologist selected seven relevant types of tissue which are identified and analyzed during the biopsy routine of breast cancer pathology (Table. 1).

To alleviate the burden of manual annotation and save time and effort for the pathologist to produce ground truth masks, firstly the annotation of the whole images was performed by a non-expert with basic knowledge of the breast cancer histology. During this process, super-pixels were created using the multi-resolution segmentation function provided by the image analysis environment *Definiens Developer XD* software, and often, there was manual intervention to modify the shape of the super-pixels in order to obtain an annotation as accurate as possible. Then, each super-pixel was manually labeled with the corresponding type of tissue. Afterwards, an expert pathologist validated and corrected the wrongly classified tissues to finally produce the ground truth multi-class masks (Figure. 1). We obtained 11 whole-slide images which have been validated by an expert pathologist. It should be noted that 6 hours are required to annotate an entire breast cancer slide with

7+Background classes and about 2 hours for validation, which underlines the tedious and time-costly nature of this task.



■ Invasive carcinoma ■ Carcinoma *In situ* ■ Benign epithelium ■ Simple stroma ■ Complex stroma ■ Adipose tissue ■ Background

Figure 1: (A) is an example of whole-slide pathological image (I1) from the dataset and (B) is its respective manual annotation provided by an expert pathologist.

### 3 A FRAMEWORK FOR TISSUE SEGMENTATION

#### 3.1 Overview of the Framework

The breast cancer segmentation approach we developed adopts an end-to-end convolutional neural network framework (Figure. 2). In this paper, we have implemented a machine learning workflow for multi-class segmentation applied on new WSI images which can be divided into several steps:

1. Pre-processing: all images are normalized to reduce the color variability within the dataset.
2. Learning: patches are randomly extracted from each image of the training dataset and injected into the network adapted for multi-class semantic segmentation.
3. Prediction and reconstruction: After a close examination of the networks behaviour, we observed that the accuracy at the border area is not precise compared to the central area of the patches. To overcome this problem, we decided that the test image is downsampled by sliding windows with a fixed stride. Then, we reassemble all overlapped predicted patches by applying a pixel-wise

argmax over all the classes probabilities to obtain the whole predicted mask.

4. Evaluation: in order to understand and optimize each step of the framework, we evaluated the outcome of the framework using segmentation metrics.

In section 4, we re-evaluate each step and their associated parameters in order to characterize this complex medical task.

### 3.2 Network Architectures

Inspired from the work of (Long et al., 2015), many recent studies have shown the effectiveness of fully convolutional neural networks **FCN** for this task. As one of the most popular pixel-level classification method, the **DeepLab** models make use of the fully connected conditional random fields CRF as a post-treatment step in their work-flow to refine the segmentation result. Deeplab model overcomes the poor localization property of deep networks by combining the responses at the final FCN layer with a CRF. Introducing skip connections has been shown to improve spatial recovery in the decoding features process, and assists with gradient flow to decoder path. The segmentation network **SegNet** architecture uses these maxpooling connections to gradually recover the feature details and size thanks to its symmetrical architecture. The well-known U-shaped network **U-Net** features several steps of downsampling convolutions, followed by upsampling deconvolution layers. Unlike SegNet, whole feature maps from each downsampling layer are passed across the intermediate layers and concatenated with corresponding upsampling layers.

### 3.3 Experiments Setup

**Evaluation Metrics.** We evaluate the performance of the evaluated models by measuring the overlap between automated and manual segmentation. We use the two following segmentation metrics: the *Dice* coefficient (DC), also called the overlap F1-score, and the Jaccard index (JI). Global metrics are not always adequate evaluation measures when class occurrences are unbalanced, which is the case in most of the medical applications, since they are biased by the dominant class(es). To avoid this, the metrics above are usually evaluated per-class and their result is averaged over the number of labeled classes.

**Training and Implementation Details.** All experiments were performed using Keras with tensorflow

backend. We used same-padding in convolutional layers in all evaluated architectures so output channels have the same dimensions as the input. We also used rectified linear units (ReLU) as activation function. To reduce the number of parameters and speed up training, instead of the last fully connected layer we used a convolutional layer, with the number of feature maps equal to the number of predicted classes for the loss function based on the cross entropy.

In every evaluation, we considered up to 9 images for the training with a 20% separate validation split. We used the remaining 2 images to evaluate the models. We kept these sets of images all along this study so we could compare our models. Each model was optimized by Adam (Kingma et al., 2014) for a pre-determined number of iterations fixed arbitrarily to 10, a batch size of 5 and exponential decaying learning rate initialized at  $1e5$ . Both classifiers were trained from scratch.

## 4 PARAMETERS SETTINGS

For each step of the workflow, we evaluate the parameters and answer the challenging questions we encounter when we started to deal with the new data (see Figure 2). For our experiments, our review of the literature convinced us to explore and evaluate two of the cited above CNN models : U-Net and SegNet.

### 4.1 Variability of H&E Stained Images

**Is a Normalization Step Necessary?** Previous work (Vahadane et al., 2016; Macenko et al.; Sethi et al.) has shown that the standardization of colors brings a clear improvement in the results of image segmentation and proposed color normalization algorithms that standardize image appearance in order to minimize variability and undesirable artifacts within the image. As a pre-processing step, we applied two of the most used normalizations on pathological data: Macenko normalization, and Vahadane normalization. We chose these approaches because initial empirical results showed Macenko-normalized images obtained high discrimination between the two subtypes of cancer classes whereas Vahadane-normalized images showed high differentiation between the epithelium and non-epithelium classes. One stained image in our dataset was chosen by an expert according to the quality of its coloring to be a target image and we normalized the other images into its color appearance. After evaluation of the prediction, we observed

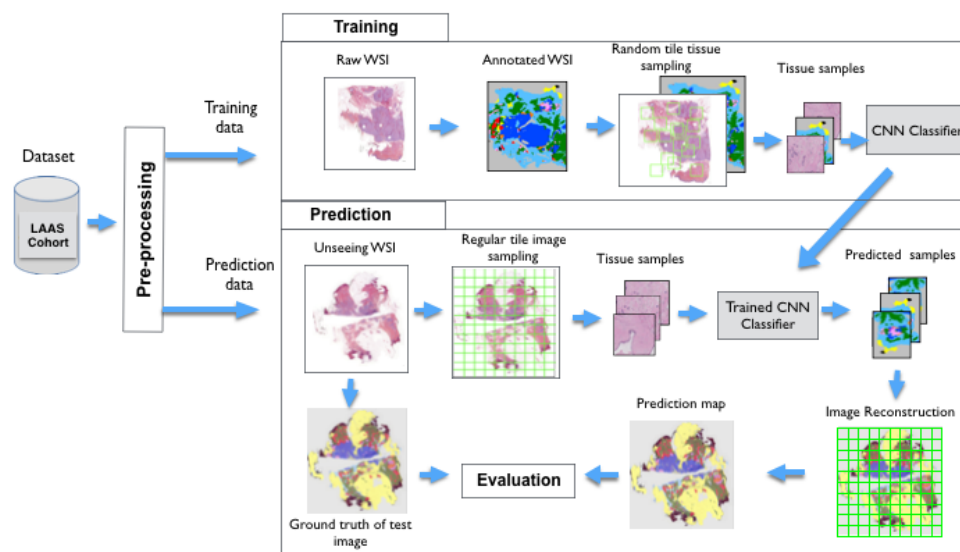


Figure 2: Workflow of the training and test phases of CNN classifiers for breast cancer image segmentation.

that both normalizations slightly improve the results, specifically the epithelium regions (Table 2).

**Does a Large Spectrum of Colors Contribute or Mislead the Learning Process?** Because of the contrast that appears more strongly in the grayscale, we wanted to evaluate how well the H&E grayscale images can improve the performance of our model. Because gray levels can facilitate the differentiation of epithelium tissue structures from non-epithelium structures. However, based on our experiments (Table 2), we found that our framework improves the identification of tissues more on raw RGB normalized images than on grayscale images. The reason could be that grayscale images miss some relevant information that might be helpful for discriminating between different tissues with similar nuclei distribution, for example invasive and *in situ* classes.

**What is the Minimum of Necessary H&E Images to Represent the Diversity of the Characterized Tissues?** In this section, we answer the following question: what the minimum amount of data to solve a semantic segmentation problem by training CNN from scratch is? This crucial question was not explored in the recent deep learning based medical image studies and in particular in image pathology publications. To address this question, we evaluated both, SegNet and U-Net, by varying the number of training images and randomly picking images from our dataset for each run. During the training phase, we observed two different behaviors: a consistent DC improvement for SegNet, as the number of training images increases whereas U-Net seems to converge

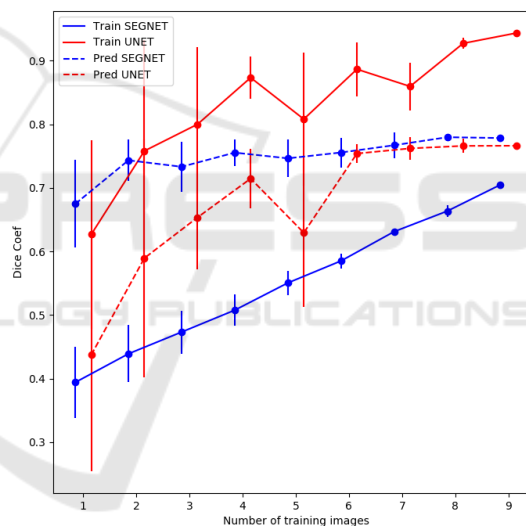


Figure 3: Comparison of different number of images on SegNet and U-Net model during the training phase and the prediction evaluation.

faster (see Figure. 3). On the opposite, during the prediction evaluation on WSIs, SegNet converges very fast to the almost optimal result, whereas U-Net needs at least 6 images to get there. The main conclusion of this observation which can be applied to any dataset for probably various domains, reveals the importance of the chosen model according to the number of inputs which is consistent with results of similar work (Ronneberger et al.). In this study we decided to keep SegNet as the optimal model as the baseline for other experiments considering that it gives better results after a training phase on 9 images.

Table 2: Quantitative comparison of 3 normalization methods applied on two test H&E images: Original (not normalized), Grayscale, Macenko and Vahadane normalizations. This table represents the pixel-wise evaluation per class and global in terms of DC and JI.

Tissues	Original		Greyscale		Macenko		Vahadane	
	JI	DC	JI	DC	JI	DC	JI	DC
IC	0.28	0.43	0.26	0.41	0.37	0.55	0.35	0.51
DCIS	0.12	0.10	0.0	0.0	0.0	0.12	0.07	0.1
Begnin epi	0.21	0.34	0.05	0.07	0.20	0.32	0.22	0.33
Stroma	0.76	0.86	0.71	0.83	0.79	0.88	0.79	0.88
Complex stroma	0.33	0.5	0.28	0.43	0.29	0.45	0.32	0.48
Adipose	0.74	0.85	0.74	0.85	0.75	0.86	0.76	0.86
Artifacts	0.25	0.39	0.19	0.33	0.30	0.45	0.28	0.43
Background	0.95	0.97	0.95	0.97	0.96	0.97	0.96	0.97
<b>Global</b>	<b>0.74</b>	<b>0.85</b>	<b>0.73</b>	<b>0.84</b>	<b>0.77</b>	<b>0.87</b>	<b>0.78</b>	<b>0.88</b>

Table 3: Dice Coefficient(DC) evaluation per tissue for 2 test images (I1 & I2) with 9 training images using four different segmentation neural networks.

Tissues	U-Net		SegNet		FCN		DeepLab	
	I1	I2	I1	I2	I1	I2	I1	I2
	DC	DC	DC	DC	DC	DC	DC	DC
IC	0.72	0.39	0.57	0.43	0.66	0.33	0.65	0.39
DCIS	0.02	0.0	0.13	0.0	0.07	0.0	0.01	0.07
Begnin epi	0.51	0.11	0.53	0.16	0.50	0.10	0.54	0.19
Simple stroma	0.84	0.90	0.85	0.90	0.83	0.89	0.85	0.90
Complex stroma	0.41	0.58	0.40	0.53	0.32	0.57	0.37	0.55
Adipose	0.88	0.81	0.88	0.85	0.87	0.82	0.87	0.82
Artifacts	0.41	0.30	0.42	0.51	0.13	0.24	0.40	0.48
<b>Global</b>	<b>0.86</b>	<b>0.86</b>	<b>0.87</b>	<b>0.88</b>	<b>0.86</b>	<b>0.86</b>	<b>0.86</b>	<b>0.87</b>

## 4.2 Optimal Tilling for Large Images

**How Much Data Augmentation Improves the Learning Process?** In a segmentation learning task, data augmentation consists of applying various image transformations simultaneously on the raw images and the validated images. In order to preserve breast tissue characteristics we avoided transformations that cause texture deformation (like shearing, mirroring). H&E images are obviously invariant by rotation, and thus we first considered the rotation transformation. In this paper, we applied a slightly different method in this study which consists in simultaneously extract and rotate the original sample at random angles. This method allows rotation-invariance and prevents over-fitting of the model. We evaluated the impact of this rotation augmentation method and we did not observe any improvement during the training (DC=0.706 with rotation and DC=0.703 without). However, when evaluating the 2 test WSIs, the improvement using the data augmentation based on rotation is very important (DC=0.876 with rotation and DC=0.433 without). Secondly, we applied elastic deformations (Simard et al., 2003) to the original extracted training samples. We chose this particular

type of deformation because it seemed to be the most adequate to represent the natural variation of texture among the tissues. Due to the large number of patches ( $N_p = 5000$ ) extracted from the raw images, we observed that elastic deformation did not improve the learning process either during the training phase or the prediction evaluation. This study confirms the importance of an appropriate data augmentation approach, and considering the large dimension of our WSIs, the overlap of patches extracted from each image combine with rotation is sufficient for data augmentation.

### What the Minimum Amount of Labeled Data is?

We evaluated two correlated parameters which are the size  $S_p$  and the number  $N_p$  of randomly extracted patches per WSI. Regarding the size of patches, we looked at a large range from 96 to 384 pixels, using  $R$  as a ratio where  $S_p = 96 * R$  with  $R \in \{1, 2, 3, 4\}$ . Figure. 4 shows the train and prediction DC of our 2 chosen networks. Obviously, both models demonstrate different behavior when  $S_p$  and  $N_p$  vary. SegNet shows a constant increase of training curve because its architecture includes batch normalization. But, starting from  $N_p = 2500$ , the DC remains con-

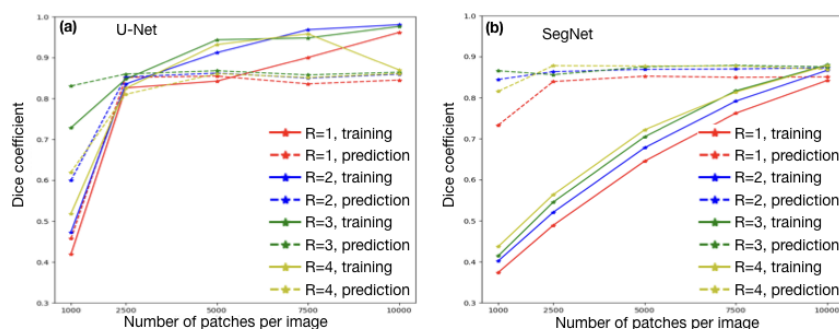


Figure 4: The train accuracy over number of training samples per image and sample size of two classifiers: (a) U-Net and (b) SegNet.

stant. A larger random samples could lead to a lot of redundancy due to overlapping patches. Secondly, there is a trade-off between localization accuracy and the use of context. Larger patches require more max-pooling layers that reduce the localization accuracy, while small patches allow the network to see more details but only little context.

## 5 RESULTS

Among the 11 WSIs in our data set, we choose two representative WSIs for test (Figure. 1) to evaluate the final prediction performance of our framework. Table 3 shows global as well as class-wise performance on the test images of the four networks predictions for the 8 classes as presented in Section 3. Even if the global score of the entire images do not vary much, SegNet slightly outperforms the other networks. Thus, giving the diversity and the number of tissue categories, it is more interesting to analyze the classes-wise metrics (Table 3) to capture the difference between the evaluated models. The class-wise accuracy clearly shows that larger classes have reasonable accuracy and smaller classes have lower accuracy. Epithelium classes and, in particular, the two carcinoma subtypes are more challenging for the models to segment than the non-epithelium classes, many of which occupy a small part of the whole image and appear infrequently as shown in Figure. 4. It is important to emphasize that U-Net displays better performance on invasive carcinoma IC where SegNet was surpassed by 15%, FCN by 8% and DeepLab by 9% respectively in terms of DC score.

**Visual Results.** Figure 5 shows the visual results of our framework with optimal setting using the four models. Even if we examined two test images with roughly equal DC and JI scores, we obtained different segmentation qualities.

## 6 CONCLUSIONS & DISCUSSION

We proposed an end-to-end framework for a medical multi-classes segmentation task. We first introduced a dataset of 11 H&E stained breast cancer images captured at intermediate resolution (20x magnification). We annotated WSIs into 7 tissues plus background categories that an expert pathologist determined important for the medical task. We proposed a deep analysis of network settings for image segmentation in order to determine the optimal configuration that can be used in similar task. The final results was evaluated using pixel-wise metrics. Results of U-Net, SegNet, FCN and DeepLab got comparable scores with DC of 0.86, 0.87, 0.86 and 0.86 respectively. The current study retains several limitations that we want to address in future work: Epithelium classes and artifacts remains a challenge to be detected due to the huge tissue variability among the WSIs. This may be improved with larger datasets and class distribution aware labeling training techniques. A reason for poor performance of carcinoma classes prediction could lie in the encoder-decoder architecture. More network architectures that capture the epithelium details may improve the segmentation performance. A new metric is necessary to reflect the medical information since the classical metrics capture the detection quality without taking into account the importance of some classes over the others.

## REFERENCES

- Aresta, G., Araújo, T., and Kwok (2018). Bach: Grand challenge on breast cancer histology images.
- Badrinarayanan, V. and Kendall (2017). Segnet: A deep convolutional encoder-decoder architecture for image segmentation. *IEEE transactions on pattern analysis and machine intelligence*.
- Beck, A. H., Sangoi, A. R., and Leung (2011). Systematic

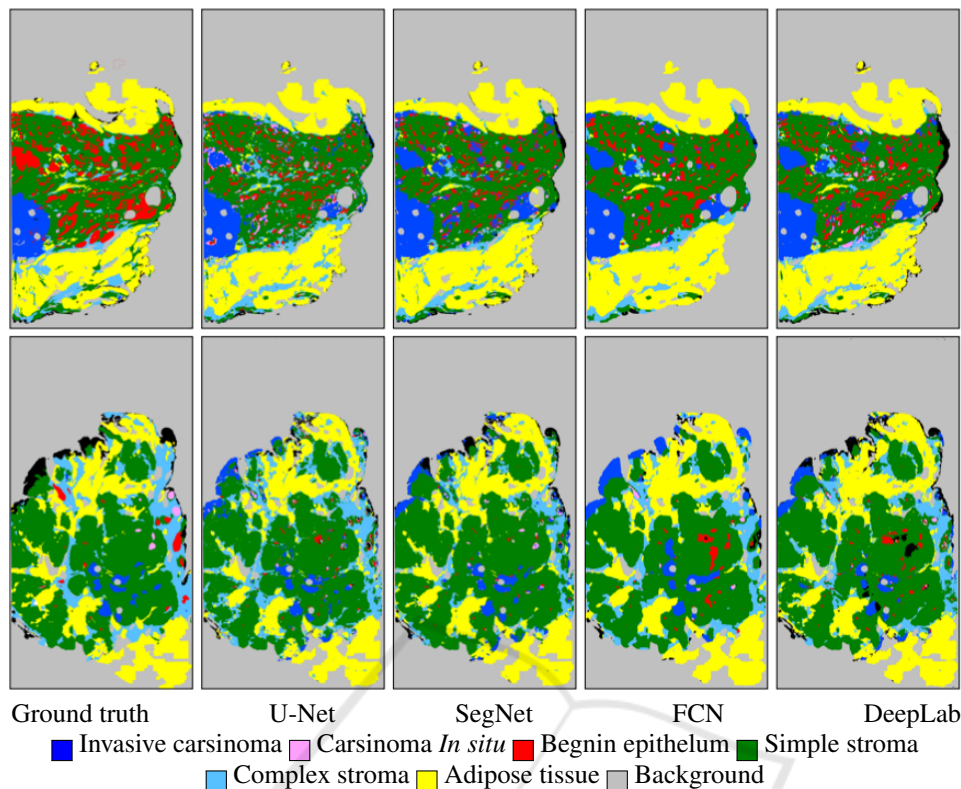


Figure 5: From left to right, two test ground truth masks, U-Net, SegNet, FCN and DeepLab multi-classes segmentation results using optimal parameters.

analysis of breast cancer morphology uncovers stromal features associated with survival. *Science translational medicine*.

Chen, H., Qi, X., Yu, L., and Heng, P.-A. (2016a). Dcan: Deep contour-aware networks for accurate gland segmentation. In *Proceedings of the IEEE conference on Computer Vision and Pattern Recognition*, pages 2487–2496.

Chen, L.-C., Papandreou, G., Kokkinos, I., Murphy, K., and Yuille, A. L. (2016b). Deeplab: Semantic image segmentation with deep convolutional nets, atrous convolution, and fully connected crfs.

Cruz-Roa, A., Gilmore, H., and et al, B. Accurate and reproducible invasive breast cancer detection in whole-slide images: A deep learning approach for quantifying tumor extent. *Scientific reports*.

Hou, L., Samaras, D., Kurc, T. M., Gao, Y., Davis, J. E., and Saltz, J. H. (2016). Patch-based convolutional neural network for whole slide tissue image classification. In *Proceedings of the IEEE Conference on Computer Vision and Pattern Recognition*.

Janowczyk, A. and Madabhushi, A. (2016). Deep learning for digital pathology image analysis: A comprehensive tutorial with selected use cases. *Journal of Pathology Informatics*.

Kingma, D. P., Ba, J., et al. (2014). Adam: A method for stochastic optimization.

LeCun, Y., Bengio, Y., and Hinton, G. Deep learning. *nature*.

Long, J., Shelhamer, E., and Darrell, T. (2015). Fully convolutional networks for semantic segmentation. In *Proceedings of the IEEE conference on computer vision and pattern recognition*, pages 3431–3440.

Loukas, C, K. (2013). Breast cancer characterization based on image classification of tissue sections visualized under low magnification. *Computational and mathematical methods in medicine*.

Macenko, M., Niethammer, M., Marron, J. S., et al. A method for normalizing histology slides for quantitative analysis. In *Biomedical Imaging: From Nano to Macro, 2009. ISBI'09. IEEE International Symposium on*.

Ronneberger, O., Fischer, P., and Brox, T. U-net: Convolutional networks for biomedical image segmentation. In *International Conference on Medical image computing and computer-assisted intervention*.

Sethi, A., Sha, L., Vahadane, et al. Empirical comparison of color normalization methods for epithelial-stromal classification in h and e images. *Journal of pathology informatics*.

Simard, P. Y., Steinkraus, D., Platt, J. C., et al. (2003). Best practices for convolutional neural networks applied to visual document analysis.

Spanhol, F. A., Oliveira, L. S., Petitjean, C., and Heutte, L. A dataset for breast cancer histopathological im-



age classification. *IEEE Transactions on Biomedical Engineering*.

Torre, L. A., Siegel, R. L., Ward, E. M., and Jemal, A. (2016). Global cancer incidence and mortality rates and trends—an update. *Cancer Epidemiology and Prevention Biomarkers*.

Vahadane, A., Peng, T., Sethi, A., Albarqouni, et al. (2016). Structure-preserving color normalization and sparse stain separation for histological images. *IEEE transactions on medical imaging*.

Wang, D., Khosla, A., Gargeya, R., Irshad, H., and Beck, A. H. (2016). Deep learning for identifying metastatic breast cancer. *arXiv preprint arXiv:1606.05718*.

